INSTITUTE OF PHYSICS PUBLISHING METROLOGIA

Metrologia **41**(2004) 376–386 PII: S0026-1394(04)85654-8

Phasevariationsinmicrowavecavitiesforatomic clocks

RuoxinLiandKurtGibble

Department of Physics, The Pennsylvania State University, University Park, PA 16802, USA

Received 11 June 2004 Published 4 October 2004 Online at stacks.iop.org/Met/41/376 doi:10.1088/0026-1394/41/6/004

Abstract

We analyse the phase variations of the microwave field in a TE_{011} microwave cavity and how these variations affect the frequency of an atomic clock. We analytically solve for the microwave fields in a TE_{011} cavity. These analytic solutions show significant new terms that are not present in previous two-dimensional treatments. The new terms show that cavities with small radii, near 2.1 cm for a 9.2 GHz cavity, have smaller phase shifts than cavities with larger radii. We also show that the three-dimensional phase variations near the axis of the cavity can be efficiently calculated with a rapidly converging series of two-dimensional finite element calculations. The cavities used in atomic clocks have holes in the endcaps, and we use finite element methods to study the large fields and phase shifts near these holes. The effects of the phase variations on atoms traversing a cavity are analysed using the sensitivity function, and we present a cavity design that has small phase shifts for all atomic trajectories. For two $\pi/2$ pulses, the proposed cavity has transverse variations of the effective phase that are within ± 0.1 μrad and produce no systematic frequency error for a nearly homogeneous and expanding cloud of atoms.

1.Introduction

In the current generation of laser-cooled atomic fountain clocks, accuracies have advanced to near and beyond 10^{-15} [1]. A number of systematic errors limit the accuracy of these and future clocks. One of the potential errors arises because the phase of the microwave field that excites the atoms is not constant throughout the microwave cavity [2]. The most common microwave cavity in fountain clocks is a cylindrical TE_{011} cavity because it has small losses (high Q) and a useful field geometry. DeMarchi and collaborators have studied several aspects of this cavity [3–5]. In [4] they show that the losses in the conducting walls of the microwave cavity imply that there is a small travelling wave component, in addition to the large standing wave. The superposition of these two fields can be viewed as a field with a small spatially varying phase shift. Because the phase of the field is different for different atomic trajectories through the cavity, a clock may have a frequency error due to this distributed cavity phase shift. DeMarchi and collaborators studied the transverse phase variations due to the sidewall losses using two-dimensional finite element calculations that assumed no variation of the fields along the axis of the cavity [4, 5]. Here, we use analytic and finite element techniques and find new terms due to three-dimensional effects. We study a number of aspects of this problem and present a cavity design that reduces, and even eliminates, effects due to the phase variations.

Our approach is to first analytically solve for the three-dimensional phase variations due to the losses in a cylindrical cavity. These analytic calculations result in simple expressions for the phase in cylindrical cavities and can guide us to better cavity designs. We then apply finite element methods and show that an azimuthal series of two-dimensional finite element calculations can efficiently produce the three-dimensional phase distributions for cavities with arbitrary shapes. Because the atoms pass through the centre of the cavity, only two to four two-dimensional calculations are required. Compared with full three-dimensional finite element calculations [6], two-dimensional calculations require much less computing resources. Computing time is reduced from hours to seconds on current desktop computers. Finally, we consider the effects of the spatial phase variations on the atoms and present an improved cavity design.

2. Analytic calculation of phase variations

In this section we present an analytic calculation treating a cylindrical cavity with no holes in the endcaps. We begin by solving for the fields of a TE_{011} cylindrical cavity that has lossy (copper) sidewalls and perfectly conducting endcaps. We then treat the endcap losses for a cavity that has perfectly conducting sidewalls. The superposition of these two solutions is the full solution for a cylindrical cavity with metallic surfaces.

The total electromagnetic field in the cavity satisfies the wave equations:

$$\left(\nabla^2 + \frac{\omega^2}{c^2}\right)\vec{H}(\vec{r}) = 0, \qquad \left(\nabla^2 + \frac{\omega^2}{c^2}\right)\vec{E}(\vec{r}) = 0, \tag{1}$$

where an $e^{-i\omega t}$ time dependence is assumed for all fields. We perturbatively expand the fields as in [4]. In a standing wave basis, the total field can be written as a superposition of a large standing wave $\vec{E}_0(\vec{r})$ and $\vec{H}_0(\vec{r})$, which satisfy the wave equations (1) with perfectly conducting walls, and small standing waves $\vec{f}(\vec{r})$ and $\vec{g}(\vec{r})$ that are also solutions of equations (1) and account for the losses.

$$\vec{H}(\vec{r}) = \vec{H}_0(\vec{r}) + (1+i)\vec{g}(\vec{r}), \qquad \vec{E}(\vec{r}) = i\vec{E}_0(\vec{r}) - (1-i)\vec{f}(\vec{r}). \tag{2}$$

While all the fields are generally complex, equations (2) are written so that $\vec{E}_0(\vec{r})$, $\vec{H}_0(\vec{r})$, $\vec{f}(\vec{r})$, and $\vec{g}(\vec{r})$ may also be real. In cylindrical coordinates $\vec{r} = (r, \phi, z)$, we take the primary TE_{011} field to be

$$\vec{E}_0(r,z) = \frac{\mu_0\omega}{2}\frac{k_1}{\gamma_1}J_1(\gamma_1 r)\cos(k_1 z)\hat{\phi}$$
$$\vec{H}_0(r,z) = \frac{k_1}{2}\left(\frac{k_1}{\gamma_1}J_1(\gamma_1 r)\sin(k_1 z), 0, J_0(\gamma_1 r)\cos(k_1 z)\right), \tag{3}$$

where, for the TE_{mnp} mode, $k_p = p\pi/d$, $\gamma_p = \sqrt{\omega^2/c^2 - k_p^2}$, $p = 1, 2, 3, \ldots$, R is the radius of the cavity, $J_m(x)$ is the Bessel function of the first kind, and the z component of $\vec{H}_0(r,z)$ is normalized so that $\int_{-(d/2)}^{d/2} H_{0,z}(0,z)\,dz = 1$ with the endcaps at $z = \pm d/2$.

2.1. Sidewall losses

To demonstrate an analytic calculation of the phase of $H_z(\vec{r})$, we consider a cylindrical cavity with sidewall losses and perfectly conducting endcaps that is fed by one or more infinitesimally small power feeds at $z = 0$, the cavity midsection. To solve for $\vec{f}(\vec{r})$ and $\vec{g}(\vec{r})$, we start with the boundary conditions for a locally uniform wave incident on a conductor. The electric field on the surface of the conductor is $\vec{E}_\parallel(\vec{r}) = (1-i)((\mu_0\omega\delta)/2)\hat{n} \times \vec{H}_0(\vec{r})$, where the skin depth is $\delta = \sqrt{2/\mu_0\omega\sigma}$, the conductivity of copper is $\sigma = 5.8 \times 10^7\ \Omega^{-1}\,m^{-1}$, $\hat{n}$ is normal to the metallic surface, and second order and higher terms in δ are neglected [4]. From this, we get the boundary condition for $f_\phi(\vec{r})$ and the power loss at all positions on the sidewalls, excluding the feed(s):

$$\vec{S} = \frac{1}{2}\mathrm{Re}(\vec{E} \times \vec{H}^*) = -\frac{1}{2}f_\phi(\vec{r})H^*_{0,z}(R,z)\hat{r} = \frac{\mu_0\omega\delta}{4}|H_{0,z}(R,z)|^2\hat{r}. \tag{4}$$

The value of $f_\phi(\vec{r})$ at the feed(s) is such that the proper power is supplied to the cavity.

We solve for $\vec{f}(\vec{r})$ and $\vec{g}(\vec{r})$ by decomposing the above boundary condition for $f_\phi(\vec{r})$ in a Fourier series of $\cos(m\phi)$ and $\cos(k_p z)$. The series is an even function of z and even in ϕ about the feed position(s) due to the symmetry of the primary field and the cavity feeds.

This Fourier decomposition of the boundary condition and the solutions $\vec{f}(\vec{r})$ and $\vec{g}(\vec{r})$ gives a helpful physical picture of power flow and phase gradients in cavities. For example, the azimuthally symmetric $m = 0$ mode can be physically visualized as a circular feed that surrounds the cavity. Because the power fed into the cavity through the sidewalls is equal to all the losses, the net $m = 0$, $p = 1$ power is zero and therefore this mode is not present in $\vec{f}(\vec{r})$ and $\vec{g}(\vec{r})$. Indeed, this mode is the primary TE_{011} field for perfectly conducting walls, $\vec{E}_0(\vec{r})$ and $\vec{H}_0(\vec{r})$, and it cannot lead to power flow into or out of the cavity.

Next we consider the $m > 0$, $p = 1$ modes of $\vec{f}(\vec{r})$ and $\vec{g}(\vec{r})$. Physically, these modes feed power into the cavity at $\phi = 0$ over the entire height of the cavity and have z dependence of $f_{\phi,m,p}(\vec{r}) = f_{\phi,m,p}(r)\cos(m\phi)\cos(k_1 z)$. Thus, if the feed is essentially $\delta(\phi)$, then all $m > 0$, $p = 1$ modes are excited equally and these construct a narrow feed at $\phi = 0$ and an equal amount of losses at all other ϕ. With this picture, the $m = p = 1$ mode represents power that is fed into the cavity over the entire height of the cavity and, in ϕ, represents power fed into the cavity for $-\pi/2 < \phi < \pi/2$ and power leaving the cavity due to wall losses for $\pi/2 < \phi < 3\pi/2$. Higher m modes further redistribute this power as a function of ϕ. For $p > 1$, these modes redistribute the power on the sidewalls to construct a narrow feed in z, which have most commonly been at $z = 0$. Considering the $m = 1$, $p = 3$ mode, it feeds power into the cavity at $-\pi/2 < \phi < \pi/2$ and $z = 0$ and feeds power to the walls for $z \approx \pm d/3$.

With this picture it is straightforward to solve the wave equation for $\vec{f}(\vec{r})$ with the boundary condition (4), and we give the solution in the appendix. Atomic clocks are principally sensitive to the phase of $H_z(\vec{r})$, which is $\Phi = -\tan^{-1}[\mathrm{Im}(H_z(\vec{r}))/\mathrm{Re}(H_z(\vec{r}))] = -g_z(\vec{r})/H_{0,z}(\vec{r})$, to lowest order in δ where $H_{0,z}(\vec{r})$ is real. With the solution for $\vec{f}(\vec{r})$, we use $\vec{g}(\vec{r}) = \vec{\nabla} \times \vec{f}(\vec{r})/\mu_0\omega$ to get $g_z(\vec{r})$:

$$g_z(\vec{r}) = \sum_{m=0}^{\infty}\sum_{p=1+\delta_{m,0}}^{\infty} g_{z,m,p}(\vec{r})$$
$$g_{z,m,p}(\vec{r}) = -\frac{\delta k_1\gamma_p}{2}\frac{1-(-1)^p}{2(1+\delta_{m,0})}\frac{J_0(\gamma_1 R)}{J'_m(\gamma_p R)}J_m(\gamma_p r) \times \cos(m\phi)\cos(k_p z), \tag{5}$$

where $J'_m(x) = dJ_m(x)/dx$ is dimensionless, $\delta_{m,j}$ is a Kronecker delta function, and only odd p modes are excited if the cavity is fed symmetrically about $z = 0$. Although γ_p is purely imaginary for large p, this $g_{z,m,p}(\vec{r})$ is real because

the modified Bessel function $I_m(x) = \mathrm{i}^{-m} J_m(\mathrm{i}x)$. To lowest order in δ, the phase is

$$\Phi(\vec{r}) = \sum_{m=0}^{\infty} \sum_{p=1+\delta_{m,0}}^{\infty} \delta\gamma_p \times \frac{1-(-1)^p}{2(1+\delta_{m,0})} \frac{J_0(\gamma_1 R)}{J'_m(\gamma_p R)} \frac{J_m(\gamma_p r)}{J_0(\gamma_1 r)} \frac{\cos(k_p z)}{\cos(k_1 z)} \cos(m\phi). \quad (6)$$

This analytic sum for $\Phi(\vec{r})$ is particularly useful because the series converges very quickly in the region of interest for atomic clocks. In the usual configuration for a TE_{011} clock cavity, all atoms traverse the cavity within a few millimetres of the z-axis since there are holes centred on the endcaps, which have a radius of order $r_a = 0.5\,\mathrm{cm}$, much smaller than the cavity radius, R. For small r, $J_m(\gamma_p r) \approx \gamma_p^m r^m / 2^m m!$, which is very small for small r and large m. Therefore, only a few azimuthal modes contribute significantly to the phase near the centre of the cavity. The lowest orders in the Taylor expansion of equation (6) dominate.

$$\frac{J_m(\gamma_p r)}{J_0(\gamma_1 r)} \approx \frac{\gamma_p^m r^m}{2^m m!} \left[1 + \frac{r^2}{4}\left(\gamma_1^2 - \frac{\gamma_p^2}{m+1}\right)\right]. \quad (7)$$

For large p, γ_p is imaginary, and so $J'_m(\gamma_p R) \propto \mathrm{i}^m\, \mathrm{e}^{|\gamma_p| R}$ grows very quickly. Further, as we show below, the effects are smaller because of their cosine dependence with z; for $p = 3$, at $z \approx 0$ the phase shift has the opposite sign as for $z \approx \pm d/3$, and so the average phase on a cavity traversal due to this term is smaller than its peak phase shift.

In table 1 we show simple polynomial expressions for each term of the cavity phase from equations (6) and (7) for a cavity with a radius of 3 cm. For two feeds, the phase is given by the sum over $m = 2, 4, 6, \ldots$. From table 1 it is clear that cavities with two or more symmetric feeds have much smaller phase gradients. Two or more feeds eliminate the large, nearly linear phase gradient at the centre of the cavity, which results from transmitting power from the feed on one side of the cavity to the walls on the other side [4, 5]. With two feeds, the largest contribution is a quadrupole phase gradient due to power flowing in near $\phi = 0$ and π and flowing out at $\phi = \pm\pi/2$. Thus, the dominant phase behaviour is $\Phi(\vec{r}) = (34\,\mu\mathrm{rad}) r^2 \cos(2\phi)$, where r is in centimetres. For four feeds, only $m = 4, 8, 12, \ldots$ terms contribute, and here, only the $m = 4$, $p = 1$ term is significant, and so $\Phi(\vec{r}) \propto r^4 \cos(4\phi)$ [5]. However, as we show next, the endcap losses lead to terms that are azimuthally symmetric (e.g. $\Phi(\vec{r}) \propto r^2$) and larger than this term. The azimuthally symmetric terms cannot be reduced by using a large number of feeds at the cavity midsection.

Table 1. Contributions to the phase near the centre of the cavity in microradians from equations (6) and (7), where r is in centimetres for a cavity resonant at 9.2 GHz with a radius of $R = 3$ cm. The $p = 3$ terms are given at $z = 0$. At $r = 0.5$ cm, summing over all terms, the phase is $\Phi = 35.8\,\mu\mathrm{rad}$ at $\phi = 0$ and $-17.7\,\mu\mathrm{rad}$ at $\phi = \pi$.

m	$p = 1$	$p = 3$
0	0	$0.004 + 0.02r^2$
1	$56.2r + 11.5r^3$	$0.02r$
2	$34.4r^2 + 9.4r^4$	$0.02r^2$
3	$-20.9r^3 - 6.4r^5$	$0.01r^3$
4	$-1.60r^4 - 0.5r^6$	$0.01r^4$

2.2. Endcap losses

We now treat a cavity with perfectly conducting sidewalls and lossy endcaps. The losses on the endcaps at $z = \pm d/2$ in a cylindrical TE_{011} cavity are given by an analogue to equation (4):

$$\vec{S} = \frac{1}{2} f_\phi(\vec{r}) H^*_{0,r}\left(r, \pm\frac{d}{2}\right)\hat{z} = \pm\frac{\mu_0\omega\delta}{4}\left|H_{0,r}\left(r, \pm\frac{d}{2}\right)\right|^2 \hat{z}. \quad (8)$$

This gives the boundary condition for $f_\phi(r, d/2)$. On the endcap, $f_\phi(r, d/2)$ is therefore proportional to $H_{0,r}(r, d/2)$: a pure excitation of the TE_{01} waveguide mode. Thus power is transmitted to the endcaps by propagation along the cylindrical waveguide section.

To begin, it is simplest to consider feeding such a cavity with a feed that is the entire height of the cavity ($p = 1$ from the preceding subsection) and azimuthally symmetric ($m = 0$). This 'cavity' therefore has no sidewalls but only lossy endcaps. Nonetheless, Maxwell's equations hold and the fields we seek obey the boundary conditions of this 'cavity'. To solve for $\vec{g}(\vec{r})$, we look first at the total solution, $\vec{E}(\vec{r})$. We take the known solution for $\vec{E}(\vec{r})$ and then subtract from it the solution for $\vec{E}_0(\vec{r})$ from equation (3) to yield $\vec{f}(\vec{r})$, from which we calculate $\vec{g}(\vec{r})$.

The known solution for $\vec{E}(\vec{r})$ extends a skin depth δ into the endcaps. Therefore $\vec{E}(\vec{r})$ has less curvature in the longitudinal direction and more curvature in the radial direction than $\vec{E}_0(\vec{r})$, the solution for perfectly conducting endcaps. To first order in δ, the $m = 0$, $p = 1$ mode is

$$\vec{E}(r, z) = \mathrm{i}\frac{\mu_0\omega}{2}\frac{k_1}{\gamma_1} J_1[(\gamma_1 + \mathrm{d}\gamma)r]\cos[(k_1 - \mathrm{d}k)z]\hat{\phi}, \quad (9)$$

where $\mathrm{d}k = k_1\delta/d$, $(\gamma_1 + \mathrm{d}\gamma)^2 = \omega^2/c^2 - (k_1 - \mathrm{d}k)^2$, and $\mathrm{d}\gamma \approx k_1\,\mathrm{d}k/\gamma_1$. Equation (9) is clearly a solution to the wave equation and one can verify that it satisfies the boundary conditions on the endcaps. We get $\vec{f}(\vec{r})$ by expanding equation (9) to first order in $\mathrm{d}k$ and $\mathrm{d}\gamma$ and then subtracting $\mathrm{i}\vec{E}_0(\vec{r})$ from it to get $\mathrm{i}\vec{f}(\vec{r})$, which is orthogonal to $\vec{E}_0(\vec{r})$. Then, $\vec{g}(\vec{r}) = \vec{\nabla} \times \vec{f}(\vec{r})/\mu_0\omega$ gives

$$g_{z,0,1}(r, z) = \frac{k_1^2\delta}{2\gamma_1 d}[\gamma_1 z J_0(\gamma_1 r)\sin(k_1 z) - k_1 r J_1(\gamma_1 r)\cos(k_1 z)] + \Phi_0 H_{0,z}(r, z), \quad (10)$$

where $\Phi_0 = (\delta/2d)[4(k_1^2/\gamma_1^2) - 1]$ is the constant phase shift that ensures that $\vec{g}_{01}(r, z)$ and $\vec{H}_0(r, z)$ are orthogonal ($\Phi_0 = 64.9\,\mu\mathrm{rad}$ for $R = 3$ cm and $d = 2.18$ cm). We again get the phase distribution in this open cavity after dividing equation (10) by $H_{0,z}(r, z)$ and give the full solutions in the appendix.

We now have to correct the power feed of this open cavity since no cavities are fed with a pure $m = 0$, $p = 1$ mode. For this, we envision a closed cavity with endcap losses and sidewalls that are perfect conductors. Equation (10) describes the $m = 0$, $p = 1$ power fed from the sidewalls to the endcaps in this cavity. To satisfy the boundary conditions on the sidewalls, we first add $p = 1, m > 0$ modes to build up the Fourier series of a narrow power feed $\delta(\phi)$ [two (four) feeds imply a sum over $m = 0, 2, 4, \ldots$ ($m = 0, 4, 8, \ldots$) modes]. The series is the same as in equations (5) and (6) except that they are multiplied by a factor of $2k_1^2 R/\gamma_1^2 d$ to account for

Table 2. Contributions to the phase near the centre of the cavity in microradians, where r and z are in centimetres for a cavity resonant at 9.192 GHz with a radius of 3 cm. The $m = 0$ and $p = 1$ term is from equations (10), and the $p = 3$ terms are given at $z = 0$. At $z = 0$ and $r = 0.5$ cm, summing over all terms, the phase is $\Phi = 134.6\,\mu\text{rad}$ at $\phi = 0$ and $-53.4\,\mu\text{rad}$ at $\phi = \pi$.

m	$p = 1$	$p = 3$
0	$32.9r^2 + 6.7r^4 - 65.8z^2$	$0.01 + 0.06r^2$
1	$197.5r + 40.3r^3$	$0.06r + 0.14r^3$
2	$120.8r^2 + 32.9r^4$	$0.07r^2$
3	$-73.5r^3 - 22.5r^5$	$0.05r^3$
4	$-5.6r^4 - 1.8r^6$	$0.03r^4$

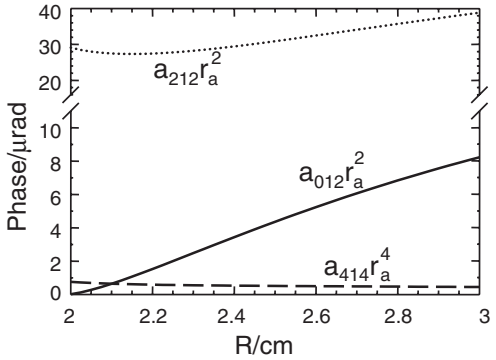

Figure 1. The magnitude of the phase of the microwave field at $r_a = 0.5$ cm due to different TE_{mp} terms, $a_{mps}r^s$, from tables 1 and 2 as a function of the cavity radius, R, for a fixed resonant frequency of 9.192 GHz. These are the leading terms for cavities with two or four feeds. Here, the leading term for the $m = 4$, $p = 1$ term is $|\phi(\vec{r})| = a_{414}r^4\cos(4\phi)$. The cavity height ranges from $d = 15.4$ cm to $d = 2.2$ cm for this range of R. For two feeds, the phase variations due to the endcap losses are smaller than the $m = 2$, $p = 1$ term. For four feeds, the phase variations due to endcap losses ($a_{012}r_a^2$) dominate for cavity radii greater than 2.1 cm.

the difference between the endcap losses in equation (10) and the sidewall losses in the previous subsection. Just as in the previous subsection, we now add the $p > 1$ modes to the $p = 1$ modes in equations (5) and (6) to reproduce a small feed $\delta(z)$ at $z = 0$, effectively representing the feeds of physical cavities.

The phase near the centre of the cavity can again be expressed as a sum of simple polynomials as in table 2. Again, the $p > 1$ modes have small effects for large cavity radii. Since the endcap and sidewall losses are of the same order, multiple feeds (e.g. at $z = 0$) generally reduce the phase variations [4, 5]. However, the $m = 0$, $p = 1$ mode that feeds the power to the endcaps produces an important phase shift. This term is present for any number of feeds on the sidewalls. The $-rJ_1(\gamma_1 r)\cos(k_1 z)$ term in equation (10) produces a phase shift $\phi(\vec{r}) = (\delta/2d)k_1^2 r^2$ that is considerable (see table 2). At first glance, the $zJ_0(\gamma_1 r)\sin(k_1 z)$ term seems to be less important as $\phi(\vec{r}) = -(\delta/d)k_1 z\tan(k_1 z)$ has no radial dependence. However, the effect of the endcap holes and the non-linear response of the atoms give it a nearly equal significance. We discuss both these further in the following sections.

2.3. Discussion of analytic results

Armed with the analytic results of the two previous subsections, we can begin to optimize the geometry of a cylindrical cavity to minimize the phase variations. The superposition of the solutions for sidewall and endcap losses gives the solution for a real cylindrical cavity. This gives the bulk of the phase shifts for a cavity with holes in the endcaps, which we treat in the following section using finite element methods.

Clearly, multiple feeds are preferable since the $m = 1$, $p = 1$ terms in tables 1 and 2 are large. With two or four feeds, the large $m = 1$ terms vanish to the extent that the feeds are the same and the conductivity and surface finish are homogeneous. In addition, phase shifts are further minimized by making sure that the modes that produce large phase shifts are detuned from the TE_{011} resonance. In equation (6), the distributed cavity phase is proportional to $1/J'_m(\gamma_p R)$, where $J'_m(\gamma_p R) = 0$ is the resonance condition. As a particular m, p mode is tuned through the TE_{011} resonance by changing the cavity geometry, the phase variations due to this mode become large, reverse, and then become smaller as $J'_m(\gamma_p R)$ goes to zero, reverses, and then grows.

Previous two-dimensional finite element treatments without endcap losses suggested using cavities with large radii and many feeds [4, 5]. Indeed, all the leading terms in table 1 decrease with increasing R, and, for m symmetrically placed feeds, $\phi(\vec{r}) \propto r^m\cos(m\phi)$ [5]. However, the endcap losses increase with R and, more importantly, produce the azimuthally symmetric phase deviations that cannot be eliminated with feeds placed at the cavity midsection. In figure 1, we show the phase shift at a distance of 0.5 cm from the cavity axis for three $p = 1$ terms as a function of the cavity radius, R. For two feeds separated by π at the midsection, the sum of sidewall and endcap losses yields a leading term $|\phi(\vec{r})| = a_{212}r^2\cos(2\phi)$ that does not change dramatically for cavity geometries near $R \approx d/2$. For four feeds, the $m = 0$ endcap loss term is an order of magnitude larger than the $m = 4$ term for $R = 3$ cm, which was analysed in [5]. These dependences suggest that cavities with radii close to $R \approx 2.1$ cm have more favourable phase distributions for atomic clocks than cavities with large radii. Below, we study such cavities and include the effects of the endcap holes using finite element methods.

To compare with previous results, we note that the two-dimensional finite element treatment of [4] is precisely the $p = 1$ case with no endcap losses. Without the endcap losses, a constant z dependence is exactly analogous to a solution where all terms have a $\cos(k_1 z)$ dependence. This corresponds to a single feed or multiple feeds that are the entire height of the cavity and narrow in ϕ. Power flow from the feeds to the walls clearly causes the phase gradients. Khursheed, Vecchi, and DeMarchi elegantly showed that, when the two-dimensional fields have no dependence on z, the transverse phase gradients are directly proportional to the transverse Poynting vector [4]. However, in three dimensions, the different k_p dependences imply that the various p terms do not add to the transverse Poynting vector and to the phase gradient in the same way. Therefore, to the extent that $p > 1$ modes are important, the relative orientation of the transverse Poynting vector and the transverse phase gradient of $H_z(\vec{r})$ can be arbitrary and vary smoothly from 0 to π. This three-dimensional behaviour shows that phase gradients and power flow are not so directly

connected and therefore suggests the possibility that power could be delivered to the cavity walls with much smaller or even no phase gradients of $H_z(\vec{r})$. One clear, albeit difficult, way of achieving infinitesimally small phase gradients is to feed a cavity with a very large number of feeds that are distributed throughout the cavity such that each feed supplies only the power that is absorbed near that feed. This is essentially exciting only very high m and p modes in addition to the primary $m = 0$, $p = 1$ mode. Below we show a simpler method of avoiding the effects of phase gradients on the atoms by choosing a cavity geometry with small phase shifts, judiciously exciting $p > 1$ modes, and considering the effects of the phase variations on the atoms.

3. Finite element model

Finite element calculations can handle complicated cavity shapes flexibly. In this section, we consider cavities that are a series of cylinders with holes in the endcaps and we study the effects of the endcaps. While these can be calculated with mode expansions [7], the finite element method, in addition to its flexibility, is more efficient because its matrices are sparse [8]. Three-dimensional finite element calculations require far more resources than two-dimensional calculations. The three-dimensional computing time scales as $T_{3D} = T_{2D}^{3/2}$ [4]; for current personal computers, this corresponds to hours versus seconds for the same geometry and mesh density in three dimensions rather than two dimensions. From the arguments in the previous section, it is clear that, for multiply fed cavities, only two two-dimensional terms in m are significant and, for a single feed, only four two-dimensional terms in m are needed for an accurate calculation of the phase distribution. In this section, we first describe our finite element calculations of three-dimensional phase distributions using a series of two-dimensional problems. We then perform a number of finite element calculations to analyse the effects of the holes in the cavity endcaps.

3.1. Two-dimensional finite element calculations

Davies *et al* [8] and others have shown that the finite element method can be applied to electromagnetic problems that have a specific azimuthal symmetry such as $\cos(m\phi)$. As in our analytic treatment above, we can decompose the boundary conditions for the losses and feeds in the cavity into a Fourier series in $\cos(m\phi)$. This leaves a series of two-dimensional problems in r and z to solve, which is far more efficient. Again, we decompose the fields into a primary standing wave and a small standing wave that accounts for the wall losses as in equation (2).

We first solve for the primary fields $\vec{E}_0(\vec{r})$ and $\vec{H}_0(\vec{r})$ in a cavity that is composed of a series of arbitrary cylinders. For the TE_{011} mode, since $m = 0$, $\vec{E}_0(\vec{r})$ has only a ϕ component. Therefore the vector wave equation in cylindrical coordinates is

$$\left[\frac{1}{r}\frac{\partial}{\partial r}\left(r\frac{\partial}{\partial r}\right) - \frac{1}{r^2} + \frac{\partial^2}{\partial z^2} + \frac{\omega^2}{c^2}\right] E_{0,\phi}(r,z) = 0, \qquad (11)$$

where $E_{0,\phi}(\vec{r}) = 0$ on the boundaries since it is parallel to every boundary. This is straightforward to implement in a finite element calculation. We then calculate $\vec{H}_0(r,z) = \vec{\nabla} \times E_{0,\phi}(r,z)\hat{\phi}/\mu_0\omega$.

The calculation for $g_{z,m}(r,z)$ with $m = 0$ follows in the same way from equation (11). The boundary condition is

$$f_\phi(\vec{r})\hat{\phi} = -\frac{\mu_0\omega\delta}{2}\hat{n} \times \vec{H}_0(\vec{r}) \qquad (12)$$

on the cavity walls, where $\hat{n}$ is the normal of the metallic surface and $\vec{H}_0(\vec{r})$ is from the above finite element calculation. To this boundary condition for the losses, we must also add the value of $f_\phi(\vec{r})$ at the cavity feed(s), which has a ϕ dependence. Integrating

$$f_{\phi,m}(\vec{r}) = \int_0^{2\pi} f_\phi(\vec{r})\cos(m\phi)\,\mathrm{d}\phi \qquad (13)$$

gives the total boundary condition, for all m, for a cavity constructed from an arbitrary number of cylindrical sections. For $m = 0$, the value of $f_\phi(\vec{r})$ at the feed must be adjusted carefully so that the net power into the cavity is zero. This eliminates an excessive amount of the primary field, $E_{0,\phi}(\vec{r})$, in the solution for $f_\phi(\vec{r})$ since an arbitrary amount of $E_{0,\phi}(\vec{r})$ satisfies the same wave equation with Dirichlet boundary conditions. As in the previous section, any residual amount of $E_{0,\phi}(\vec{r})$ is removed, so that finally $f_{\phi,0}(r,z)$ and $E_{0,\phi}(\vec{r})$ are orthogonal. Then $\vec{g}_0(r,z) = \vec{\nabla} \times f_{\phi,0}(r,z)\hat{\phi}/\mu_0\omega$.

The calculation of $\vec{g}_m(\vec{r})$ for $m > 0$ is more involved because $\vec{f}_{m>0}(\vec{r})$ has both radial and azimuthal components. Therefore the solutions must simultaneously satisfy the wave equations and $\vec{\nabla} \cdot \vec{f}_m(\vec{r}) = 0$. In the usual way, we solve the scalar wave equation for $\psi_m(r,z)$.

$$\left[\frac{1}{r}\frac{\partial}{\partial r}\left(r\frac{\partial}{\partial r}\right) - \frac{m^2}{r^2} + \frac{\partial^2}{\partial z^2} + \frac{\omega^2}{c^2}\right] \psi_m(r,z) = 0. \qquad (14)$$

Then $\vec{f}_m(\vec{r}) = -\mu_0\omega\vec{\nabla} \times [\psi_m(r,z)\cos(m\phi)]\hat{z}$ and $\vec{g}_m(r,z) = \vec{\nabla} \times \vec{f}_m(r,z)/\mu_0\omega$, so that $g_{z,m}(\vec{r}) = \nabla_{\mathrm{tr}}^2\psi_m(r,z)\cos(m\phi)$, where ∇_{tr}^2 is the transverse Laplacian.

The picture of the azimuthal expansion for our finite element method is different from that for our analytic treatment above. Here, in the two-dimensional finite element calculations, we solve for all p modes simultaneously. For example, the feed for $m = 0$ could be a short feed (a height $\Delta z = 2\,\mathrm{mm}$) that feeds power into the cavity symmetrically around the circumference at $z = 0$. Then, the $m > 0$ modes redistribute the feed around the narrow $z = 0$ feed region to construct one or more feeds that are narrow in ϕ. Thus, if the conductivity of the sidewalls is independent of ϕ, then $f_{\phi,m>0}(\vec{r}) \neq 0$ only for those values of z where power is fed. Therefore, the $m > 0$ boundary conditions only describe the redistribution of power in the transverse plane of the feed. Note that this does not imply that $\vec{g}_{z,m>0}(\vec{r}) = 0$ at all other z, only that the boundary conditions (equation (13)) are zero. To summarize, equations (13) give a boundary condition $f_{\phi,m>0}(\vec{r}) = 0$ for all z except where power is supplied. Since $f_\phi(\vec{r}) = \mu_0\omega\sum_{m=0}(\mathrm{d}/\mathrm{d}r)\psi_m(r,z)\cos(m\phi)$, $(\mathrm{d}/\mathrm{d}r)\psi_{m>0}(r,z) = 0$ on the cavity sidewalls. On the cavity endcaps, $f_{r,m}(\vec{r}) = \mu_0\omega m\psi_{m>0}(r,z)\sin(m\phi)/r$ must be 0 to first order in δ since there is no $\hat{\phi}$ component of $\vec{H}_0(\vec{r})$ to drive this current. Therefore, $\psi_{m>0}(r,z) = 0$ on the cavity endcaps.

We calculate the three-dimensional phase distribution in the cavity as $\sum -g_{z,m}(\vec{r})/H_{0,z}(\vec{r})$. Again, since $g_{z,m}(\vec{r})$ is a solution to the wave equation, $g_{z,m}(\vec{r}) \propto r^m$ for small r and therefore the Fourier series in m converges rapidly. We use a triangular lattice with as many as 50 000 triangles. Each calculation for any m takes less than 4 min on a 1.5 GHz personal computer with 1 GB of RAM. We have written our own finite element codes, and, more recently, we use commercially available finite element software that has the flexibility to specify the boundary conditions for $f_{\phi,0}(\vec{r})$ or $\psi_{m>0}(\vec{r})$ [1]. In the following, we show solutions for cavities with endcap holes and solutions with extremely dense meshing that enables us to examine the behaviour of the fields on the scale of the skin depth. In the next section, we use these methods to optimize cavity geometries.

3.2. Effects of endcap holes

The cavities for atomic fountain clocks must have holes in the cavity endcaps if the atoms are to pass through the cavity. When there are holes in the endcaps, the phase of the field does not go to $\pi/4$ as it does near the surface of the endcap as in equation (10). Therefore, the holes seem to improve the homogeneity of the phase distribution for two reasons: (1) $g_{z,0}(\vec{r})$ can be smaller over the aperture and (2) $H_{0,z}(\vec{r})$ does not go to zero at $z = \pm d/2$, as it does on the metal boundary. Instead, $H_{0,z}(\vec{r})$ extends beyond the aperture of the endcap hole and into the below-cutoff waveguide sections that prevent microwave leakage from these cavities. However, while the phase shifts are no longer so large over most of the aperture, we show that they do have a transverse variation that is large compared with the phase variation near $z = 0$.

In figure 2 we show the magnitude of $H_{0,z}(\vec{r})$ in the cavity and, in the inset, $H_{0,z}(\vec{r})$ near the wall of the endcap hole. While $H_{0,z}(\vec{r})$ does not go to zero for all $z = \pm d/2$ as it does in a cavity with no holes, a large fraction of the atomic trajectories (nominally parallel to z) with $r < r_a$ cross a node of $H_{0,z}(\vec{r})$ (shaded region in figure 2 inset) that is due to the hole in the endcap [9]. This occurs because the lowest mode excited in the below-cutoff waveguide section is the TE_{01}. Therefore $H_{0,z}(\vec{r})$ in the below-cutoff section must be reversed near the walls relative to the centre of the waveguide, and hence reversed relative to $H_{0,z}(\vec{r})$ at the centre of the cavity. Near the nodes $H_{0,z}(\vec{r})$, the phase of the field goes from 0 to $-\pi$ with a large phase chirp where the phase shift is $-\pi/4$ at the node of $H_{0,z}(\vec{r})$. Here we analyse the fields near the walls of the endcap holes. In the next section, we show a design that has much smaller phase shifts in this region.

A large current is induced in the wall of the endcap hole by the magnetic flux through the hole. Near the wall, the field is very large with a $-\pi$ phase shift. In fact, for cavity geometries near $R \approx d/2$, $H_{0,z}(\vec{r})$ is slightly greater at the corner than at the centre of the cavity. This large parallel component of $\vec{H}(\vec{r})$ near the surface implies a large loss in the conductor and therefore large phase shifts nearby. It is worth noting that, if the cavity is perfectly machined and vertical, 1% of the atoms pass within 12.5 μm of the walls of a 1 cm diameter aperture on the two passes through the cavity. The natural fountain velocity reversal and misalignments will eliminate the bulk of the effects. Nonetheless, since these atoms experience 100 times larger phase shifts than atoms near the centre, further study of these effects is clearly warranted.

[1] We have used FEMLab from COMSOL, Inc., Burlington, MA for the calculations presented here.

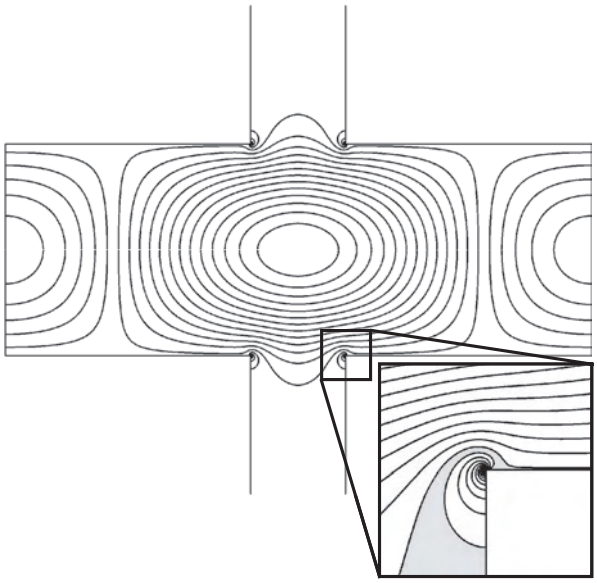

Figure 2. Contours of $H_{0,z}(\vec{r})$ for the TE_{011} mode of a cylindrical cavity with radius $R = 3$ cm, height $d = 2.176$ cm, and hole radius $r_a = 0.5$ cm. The inset is a 0.5 cm square region centred at $(r_a, \phi, -d/2)$. The shaded region in the inset contains the node of $H_{0,z}(\vec{r})$. $H_{0,z}(\vec{r})$ has local maxima at the centre of the cavity and near $r = r_a$ on the endcaps (see inset).

Within a few hundred micrometres of the corner, the fields are magnetostatic and azimuthally symmetric ($m = 0$). The wave equations (1) become Laplace's equation as ω^2/c^2 can be neglected. Because the radius of the holes in the endcaps is much greater than the skin depth, the solution near the corner is a two-dimensional problem. We transform our three-dimensional cylindrical coordinates (r, ϕ, z) to a two-dimensional problem with cylindrical coordinates such as $\rho = \sqrt{(r - r_a)^2 + (z + d/2)^2}$ and $\tan(\theta) = (z + d/2)/(r - r_a)$, for the corner on the endcap at $z = -d/2$. The solution to $\nabla^2 E_{0,\phi}(\rho, \theta) = 0$ is $E_{0,\phi}(\vec{\rho}) = a(\rho/\delta)^{2/3} \sin(\frac{2}{3}\theta) + b(\rho/\delta)^{4/3} \sin(\frac{4}{3}\theta) + \cdots$, satisfying the boundary conditions $E_{0,\phi}(\vec{\rho}) = 0$ on the conducting walls at $\theta = 0$ and $3\pi/2$. Here it is convenient to use the skin depth to make $E_{0,\phi}(\vec{\rho})$ dimensionless. For cavities with $R \approx d/2$, the antisymmetric coefficient b is about 1% of the symmetric coefficient a. From $\vec{H}_0(r, z) = \vec{\nabla} \times E_{0,\phi}(r, z)\hat{\phi}/\mu_0\omega$, we get

$$\vec{H}_0(\vec{r}) = \frac{-2}{3\mu_0\omega} \times \left[a \frac{\{r\cos(\frac{2}{3}\theta) + z\sin(\frac{2}{3}\theta), 0, -r\sin(\frac{2}{3}\theta) + z\cos(\frac{2}{3}\theta)\}}{\delta^{2/3}(r^2 + z^2)^{2/3}} + 2b \frac{\{r\cos(\frac{4}{3}\theta) + z\sin(\frac{4}{3}\theta), 0, -r\sin(\frac{4}{3}\theta) + z\cos(\frac{4}{3}\theta)\}}{\delta^{4/3}(r^2 + z^2)^{1/3}} + \cdots \right]. \quad (15)$$

This $\vec{H}_0(\vec{r})$ diverges near the corner as $\rho^{-1/3}$, just as electrostatic fields diverge with the same power laws near sharp points (e.g. lightning rods).

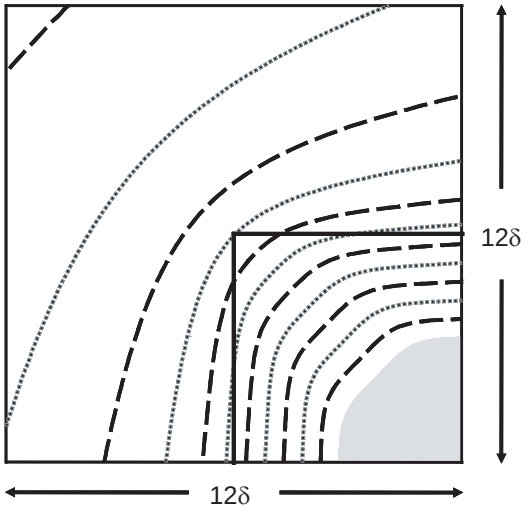

Figure 3. Contours of $\log(|E_\varphi(\vec{r})|)$ near the wall of a centred endcap hole for the TE_{011} mode. The field is smooth near the corner and falls exponentially inside the conductor. Each contour step between dashed and dotted lines represents $e^{-1/2}$. In this region the solution depends very weakly on the cavity geometry. Here, $R = 2.55\,\text{cm}$, $r_a = 0.5\,\text{cm}$, and $d = 2.6\,\text{cm}$.

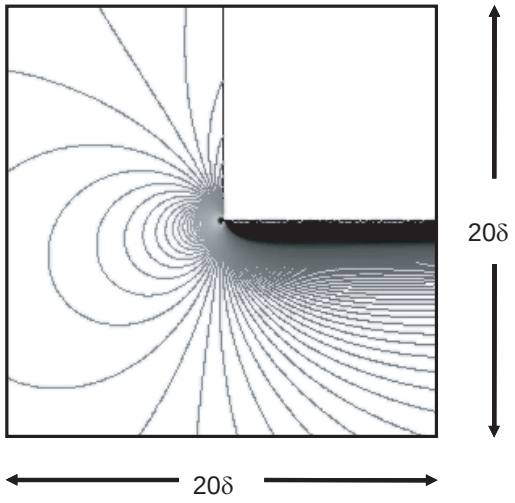

Figure 4. Contours of the phase of $H_z(\vec{r})$ near the wall of a centred endcap hole for the TE_{011} mode and the cavity of figure 3. The contour steps are 10 mrad. Within a skin depth of the corner, the phase variations are very rapid. The phase of $H_z(\vec{r})$ goes to $-\pi/4$ on the bottom surface of the top endcap.

The real $\vec{H}(\vec{r})$ cannot diverge at the corner, nor will a finite element calculation of $\vec{H}_0(\vec{r})$. On the scale of the skin depth, δ, the field must be smooth. We calculate the field near the cavity aperture using a novel finite element method. The finite element grid includes the conductor with a mesh spacing that is a fraction of the skin depth, and we simultaneously solve the coupled equations for the real and imaginary parts of the total field, $\vec{E}(\vec{r})$. The wave equations are

$$\begin{aligned}
\left(\nabla^2 + \frac{\omega^2}{c^2}\right)(E_{0,\phi}(\vec{r}) + f_{0,\phi}(\vec{r})) &= 0,\\
\left(\nabla^2 + \frac{\omega^2}{c^2}\right) f_{0,\phi}(\vec{r}) &= 0,\\
\nabla^2(E_{0,\phi}(\vec{r}) + f_{0,\phi}(\vec{r})) - \frac{2}{\delta^2} f_{0,\phi}(\vec{r}) &= 0,\\
\nabla^2 f_{0,\phi}(\vec{r}) + \frac{2}{\delta^2}(E_{0,\phi}(\vec{r}) + f_{0,\phi}(\vec{r})) &= 0.
\end{aligned} \tag{16}$$

Here the first two equations describe the vacuum region and the last two describe the decay of the fields in the metal.

We show the magnitude of $\vec{E}(\vec{r})$ near the corner of the cavity apertures in figure 3. Many skin depths away from the corner, the fields decay as $e^{-(1-i)x/\delta}$ in the metal, where x is the distance normal to the interface. Near a corner, the parallel component of $\vec{H}(\vec{r})$ approaches $\rho^{-1/3}$ up to a distance of nearly 1 mm from the corner, beyond which $\vec{H}_z(\vec{r})$ begins to follow the dominant TE_{01} waveguide mode. At distances less than a skin depth from the corner, the fields are smooth and the gradient of $\vec{E}(\vec{r})$ points nearly along the bisector of the two infinite half planes forming the two-dimensional corner. Neither $\vec{E}(\vec{r})$ nor $\vec{H}(\vec{r})$ diverges at the corner. In fact, $\vec{H}_z(\vec{r})$ is 20% smaller at the corner than at one skin depth away from the corner on the metal surface because the gradients normal to the surface in figure 3 are also slightly smaller at the corner. Therefore the local maxima of $\vec{H}_z(\vec{r})$ are about one skin depth from the corner.

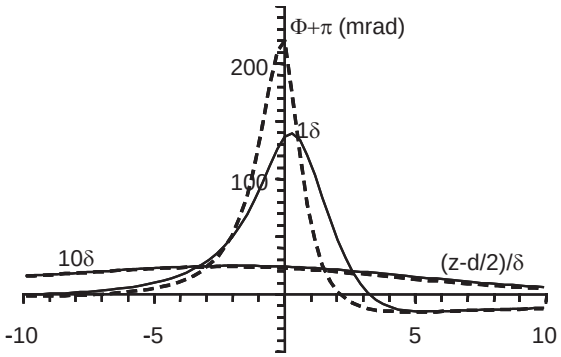

Figure 5. The phase of $H_z(\vec{r})$ of figure 4 for a vertical trajectory parallel to the z-axis and a distance of 1δ and 10δ from the wall of an endcap hole (——). The phase shifts are large near the corner at $z = d/2$. The dashed lines represent the phase as calculated using equation (4) as a boundary condition and a mesh density of four triangles per skin depth, δ.

In figures 4–6 we show the phase of $H_z(\vec{r})$ near the corner of the endcap hole. Near the corner, the phase shift is large. An atom passing within one skin depth of the corner sees the phase of the field go from $-\pi$ to $-\pi + 0.14$ and then back to $-\pi - 0.015$ within a few skin depths of the corner (figure 5). Farther away, at 10δ and 100δ from the corner, the phase variation is smaller (figures 5 and 6). In figure 6, one can also see the large phase variations experienced by all such trajectories that pass through the node of $H_{0,z}(\vec{r})$ just below $z = d/2$.

The calculations in figures 3 and 4 use a mesh density as high as 30 triangles per skin depth. Using this mesh density for the entire cavity is inefficient. To solve the problem, we divide the cavity into five overlapping subregions with increasingly higher mesh density. The solutions are iterated so that the solution and its derivative are continuous across the boundaries. The solution is well known for a plane wave incident on an infinite flat surface, and this reproduces the boundary condition (equation (12)) for much of the cavity.

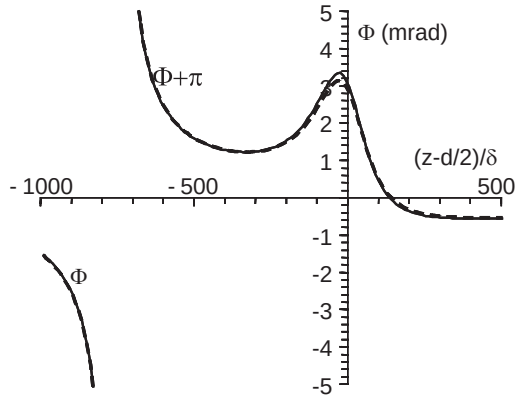

Figure 6. The phase of $H_z(\vec{r})$ of figure 4 for a vertical trajectory parallel to the z-axis and a distance of 100δ from the wall of an endcap hole (——). The phase shifts are large near the corner at $z = d/2$. Near 750δ (0.5 mm) from the corner, there is a node of $H_{0,z}(\vec{r})$ and its polarity reverses. The dashed line represents the phase calculated using equation (12) and a mesh density of four triangles per skin depth, δ. At distances much greater than δ from the surfaces, the two solutions converge.

Within a few skin depths of the corner, equation (12) is not accurate. Additionally, in the cutoff waveguide section, $H_{0,z}(\vec{r})$ does not resemble an incident plane wave. Rather, the wave falls exponentially in z, parallel to the surface. The effective surface resistance for this case is 1% to 0.3% larger, and this can change $g_z(\vec{r})$ by a larger fraction. After iterating the solution using this treatment of the metallic corner, we then solve the metallic problem for small regions in the cutoff waveguide section. From these solutions, we can determine an effective surface resistance that varies smoothly along the cutoff waveguide section. We use this effective surface resistance in turn to solve for $f_{\phi,0}(\vec{r})$.

In figures 5 and 6 we also compare our calculations of the phase with a calculation that uses the boundary condition (equation (12)). We find that the correct power is dissipated in the corner region when we choose a mesh density such that the length of a triangle side[2] is about $\delta/4$. Figure 6 shows that an atomic trajectory 100δ from the wall of the endcap hole sees a phase shift that is quite close to that calculated without properly treating the fields in the conductor. For trajectories closer to the surface, figure 5 shows that for a trajectory 1δ from the wall of the endcap hole, the fields in the conductor must be treated properly to accurately reproduce the phase shifts.

4. Improved cavities

To reduce the perturbation of the frequency of an atomic clock due to phase variations, we must first understand the effect. Although, from the previous section, the phase variations are large for cavities currently in use, here we will only treat small phase variations because the improved cavities that we suggest below have phase shifts that are everywhere less than 1 mrad for all atomic trajectories. For small phase variations, the sensitivity function [11, 12] is very useful for describing perturbative effects on the frequency of an atomic clock. In this section we develop the sensitivity function and then apply it to improving cavity designs.

[2] Here we use first order mesh elements. For most calculations where we take derivatives of the finite element solutions, we use second order mesh elements [10].

4.1. The sensitivity function

We begin with a magnetic dipole interaction Hamiltonian that leads to a Rabi frequency of $\Omega = -b_p\mu_0\mu_z H_{0,z}(\vec{r})/\hbar$, where b_p is an attenuation constant. In the rotating wave approximation, the Bloch vector evolves as [11–13]

$$\frac{\mathrm{d}}{\mathrm{d}t}\begin{pmatrix} a_1 \\ a_2 \\ a_3 \end{pmatrix} = \begin{pmatrix} 0 & 0 & 0 \\ 0 & 0 & \theta'(t) \\ 0 & -\theta'(t) & 0 \end{pmatrix}\begin{pmatrix} a_1 \\ a_2 \\ a_3 \end{pmatrix}, \qquad (17)$$

where $\theta(t) = \int_0^t \Omega(t')\,\mathrm{d}t'$, the Rabi frequency varies in time due to the atomic motion through the cavity, the microwave field is resonant with the transition frequency, and the second $\pi/2$ pulse is phase shifted by $\pi/2$. For clarity, we neglect the small effects of the variation of the atomic velocity during the cavity transit due to gravity. With an initial condition of $\vec{a} = (0,\ 0,\ -1)$, the evolution of the atoms during the first passage through the cavity is $\vec{a}(t) = \{0,\ -\sin[\theta(t)],\ -\cos[\theta(t)]\}$. The atoms leave the cavity at time $t = \tau$, where $\theta(\tau) = \pi/2$.

Small phase variations in the cavity produce small changes in the transition probabilities. The effect on the transition probability can be calculated using the sensitivity function. The sensitivity function for the first cavity passage is $s(t) = -\sin[\theta(t)]$. It is given at all other times by symmetry and continuity [12]. The change in transition probability is then

$$\delta P = \frac{1}{2}\int_0^\tau s(t)\frac{\mathrm{d}\phi(t)}{\mathrm{d}t}\,\mathrm{d}t. \qquad (18)$$

The sensitivity function has been used extensively to describe the effects on the atoms due to a stochastic evolution of the phase of a local oscillator [11]. In contrast, the phase variations in a microwave cavity evolve deterministically and, particularly because of the second passage through the cavity, the phase always returns at some time to some well known offset (e.g. the phase of the field at $z = 0$). It is therefore helpful to integrate equation (18) by parts [9]. We imagine that well outside the cavity, where $H_z(\vec{r})$ is negligibly small, the phase of $H_z(\vec{r})$ goes smoothly to the value of the phase at the centre of the cavity (which we could define as 0 without loss of generality). Therefore the surface term, $s(t)\phi(t)$, of the integration by parts is 0, giving

$$\delta P = -\frac{1}{2}\int_0^\tau \frac{\mathrm{d}s(t)}{\mathrm{d}t}\phi(t)\,\mathrm{d}t. \qquad (19)$$

Substituting $s(t)$, $\Phi(\vec{r}) = -g_z(\vec{r})/H_{0,z}(\vec{r})$, and $\mathrm{d}P(r,\phi) = \delta\Phi_{\mathrm{eff}}(r,\phi)/2$, we get the effective phase for an atom passing vertically upwards through the cavity at a transverse position (r,ϕ):

$$\delta\Phi_{\mathrm{eff}}(r,\phi) = -\frac{\pi}{2}\int_{-\infty}^{\infty}\cos[\theta(\vec{r})]g_z(\vec{r})\,\mathrm{d}z, \qquad (20)$$

where $\theta(r,\phi,z) = (\pi/2)\int_{-\infty}^{z} H_{0,z}(r,z')\,\mathrm{d}z'$.

4.2. Improved cavities

To design a better cavity, it is helpful to examine equation (20) in the context of our analytic model for a cylindrical cavity. For any $p = 1$ mode with a z dependence of $\cos(k_1 z)$, if we take $g_{z,m,p}(\vec{r}) = -\Phi_{m,p}(r,\phi)(k_1/2)J_0(\gamma_1 r)\cos(k_p z)$ and neglect the variations of the Rabi frequency with r, then the phase is independent of z throughout the cavity and the effective phase is $\delta\Phi_{\rm eff}(r,\phi) = \xi_p \Phi_{m,p}(r,\phi)$ with $\xi_1 = 1$. For $p = 3$, the effective phase is smaller than the phase at $z = 0$ and it has the opposite sign because the phase shift is larger and negative at $z = \pm d/3$. Equation (20) yields $\xi_3 = -0.217$. For higher p, $\xi_5 = 0.152$ and ξ_p decreases as $1/p$. Since $\xi_p \neq 0$ for $p > 1$, it is possible to design a cavity that appropriately excites $m = 0$, $p > 1$ modes to cancel the $m = 0$, $p = 1$ phase shifts[3]. Here, we first examine the physics of effective phase shift variations using our analytic treatment of a cylindrical cavity and then we numerically analyse cavities with holes in the endcaps. We conclude with a cavity design that has small phase variations that are carefully adjusted so that they have no effect on a cloud of atoms in an atomic clock.

Our analytic models show that using a large number of feeds distributed in ϕ eliminates the phase shifts due to $m > 0$ modes. We therefore consider four or more feeds distributed around the cavity circumference. For more than four feeds, the $m > 0$ phase variations are uninterestingly small and therefore we focus on the $m = 0$ phase shifts. In the previous paragraph, we neglected the $m = 0$, $p = 1$ $k_1 z J_0(\gamma_1 r)\sin(k_1 z)$ term of $g_{z,0,1}(r,z)$. While this term produces no transverse variation of the phase, it produces a large phase variation in z. Because the tipping angle, $\theta(r,\phi,z \gg d/2)$, is not constant for all r, the phase variation in z leads to a significant transverse variation of $\delta\Phi_{\rm eff}(r,\phi)$[4]. In figure 7, we show the $m = 0$, $p = 1$ effective phase difference between $r = 0$ and $r = 0.6$ cm. A comparison of the $m = 0$, $p = 1$ effective phase variation in figure 7 with the phase variation in figure 1 shows that the two terms in equation (10) are comparable for small R.

In figure 7 we show the effective phase variations of several important modes for cavity radii between 2 cm and 2.2 cm. There are a number of routes to eliminating the effects of the $m = 0$ phase variations. From figure 7, it seems that a cavity radius of 2.11 cm has very small effective phase variations due to the $m = 0$, $p = 1$ mode. However, we calculate the effects of the endcap holes below, and their effect is to increase the contribution of the $k_1 z J_0(\gamma_1 r)\sin(k_1 z)$ term to the effective phase. As a result, for cavities with endcap holes, the $m = 0$, $p = 1$ effective phase shift difference of figure 7 is negative for all R. Therefore, to use $p > 1$ modes to cancel the $m = 0$, $p = 1$ effective phase shift, cavity radii less than 2.2 cm are required, so that the $p > 1$ modes have phase shifts comparable with the $m = 0$, $p = 1$ mode.

To cancel the negative $m = 0$, $p = 1$ effective phase shift difference, we need a positive phase shift difference $[\Phi_{\rm eff}(0.6\,{\rm cm}) > \Phi_{\rm eff}(0)]$. Because the $m = 0$, $p = 3$ effective phase shift difference is negative, one can feed the cavity at $z = \pm d/3$ with four or more azimuthally distributed feeds. This excites the $p = 3$ modes with twice the amplitude and the opposite sign as do feeds at $z = 0$. Another possibility is to excite the $p = 5$ modes to varying degrees. The exact cavity radius and the feed positions affect the power dependences, and future work will examine these considerations.

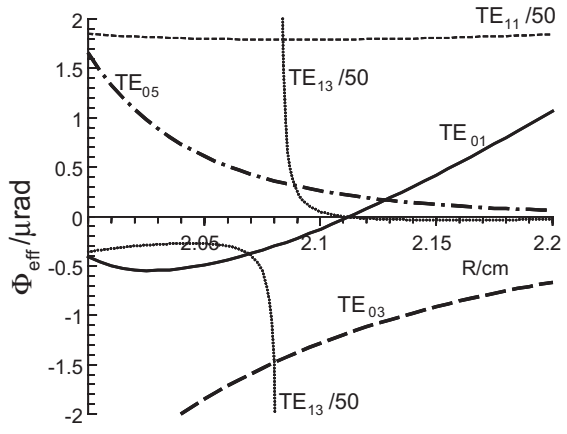

Figure 7. The difference of the effective phase shifts for an atom traversing a cavity at $r = r_{\rm a} = 0.6$ cm and $r = 0$ for various modes as a function of cavity radius, R. The cavity is resonant at 9.192 GHz and has no endcap holes. For $R = 2.11$ cm, if only the $m = 0$, $p = 1$ mode is excited, the phase shifts for all trajectories are small. The nominally unexcited $m = 1$ modes produce large phase shifts, 50 times larger than the curves depicted.

In figure 7 we also show the effective phase shift differences for two $m = 1$ modes. The $m = 1$ modes are particularly dangerous because they couple directly to an error in launch direction or tilt of the fountain. As a function of cavity radius, the $m = 1$, $p = 1$ phase shift is smallest for $R = 2.089$ cm and is 80% larger for $R \approx 3$ cm. The $m = 2$, $p = 1$ mode is also considerable (see figure 1), but its weak coupling to fountain tilt and density inhomogeneities causes less concern. We also show the $m = 1$, $p = 3$ mode because the $\rm TE_{113}$ has a nearby resonance. A small perturbation to R can easily avoid the $\rm TE_{113}$ resonance, and so the $m = 1$, $p = 3$ effects are much smaller than the $m = 1$, $p = 1$ effects. Around $R = 2.1$ cm there are a number of other TE and TM resonances that should also be avoided.

The $m = 1$, $p = 1$ term is very large because it represents power transmitted from a feed on one side of the cavity to the wall on the opposite side. One cannot fully benefit from any $m = 0$ cancellation unless the cavity losses and feeds are symmetric to better than 1%. One clear problem when constructing cavities is the evaluation of the phase shifts of unintended modes. Clairon *et al* [14] have used two independent feeds that are externally balanced to exaggerate or nominally cancel the $m = 1$ phase shifts. Our picture of phase shifts arising from individual modes shows another straightforward path to eliminating the phase variations of any mode. Using a number of feeds at $z = \pm d/3$ (but fed with a single external source), one can probe the $m = 1$, $p = 1$ and $m = 1$, $p = 3$ resonances. Small adjustments could be made to the cavity's symmetry to ensure that these are not excited. This can be done electrically, and, once the cavity is installed, the symmetry can be monitored using the ac Zeeman shift of the atoms [15].

[3] Although modes for even p are not excited, it is prudent to avoid any resonances. For even modes $\zeta_2 = -0.546$ and $\zeta_4 = 0.203$.

[4] Because the entire effect of the $k_1 z J_0(\gamma_1 r)\sin(k_1 z)$ term depends upon power variations, there is a significant power dependence. Here, we calculate $\delta\Phi_{\rm eff}(r,\phi)$ where we have adjusted the power to have a maximum of the average coherence (maximum magnitude of a_2 in equation (17)) for atoms uniformly illuminating the cavity aperture.

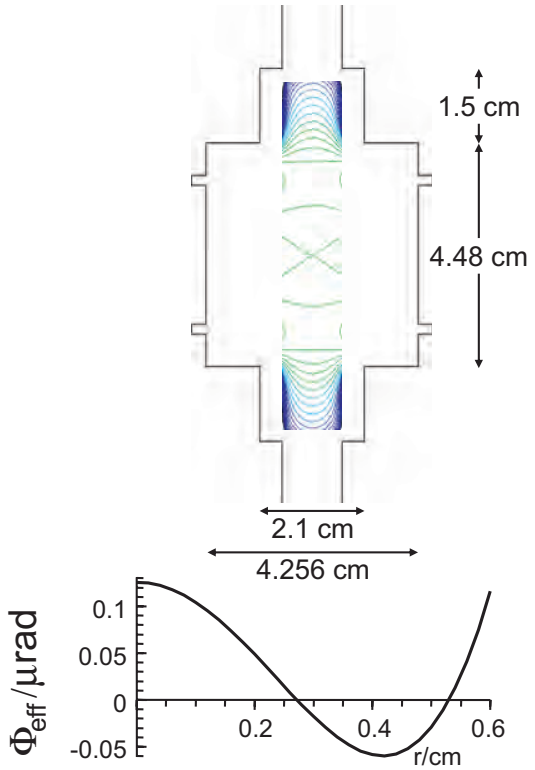

Figure 8. A cavity design with very small variations of the effective phase shifts. The cavity has a radius of $R = 2.128$ cm, and power is supplied at $z = \pm 1.487$ cm. The endcap holes are constructed with two sections of below-cutoff waveguide of diameter 2.1 cm and 1.2 cm, so that the atoms experience no nodes of $H_z(\vec{r})$ as in figure 2. The phase contours are steps of 25 μrad. The $m = 0$ effective phase shift varies by ±0.1 μrad over the 1.2 cm aperture. (This figure is in colour only in the electronic version)

In figure 8 we show a cavity and its $m = 0$ effective phase variations. The cavity is fed at $z = \pm d/3$ and has a radius of $R = 2.128$ cm. The dominant behaviour of the effective phase shifts follows those in figure 7. It is therefore critical to carefully choose the cavity radius and feed positions. The geometry of the cavity near the endcap holes is equally important. We choose a large 2.1 cm diameter cutoff wave guide section followed by a 1.2 cm waveguide section that sets the aperture of the cavity. The corner of the 2.1 cm section is relatively far from all atomic trajectories, and the diameter is such that no atoms see a node of $H_{0,z}(\vec{r})$. Therefore no atoms experience the large phase shifts near the corner as shown in figures 4–6. The 2.1 cm diameter waveguide section is sufficiently long to make $H_{0,z}(\vec{r})$ sufficiently small for the large phase shifts near the corner of the 1.2 cm section not to significantly affect the atoms.

We arrive at our cavity geometry in figure 8 after more consideration of the effect of the cavity on the sample of atoms in a clock. In an atomic fountain, atoms cooled to 1.5 μK are sufficiently hot for the mean radius of a laser-cooled sample to increase by a factor of 2 during an interrogation time of 0.5 s. If the $m = 1$ modes are not excited, a fountain tilt or a launch angle error does not produce an error. We therefore expect the dominant error due to phase gradients to be density inhomogeneities during the first passage through the cavity. We expect the density variations will be small, and

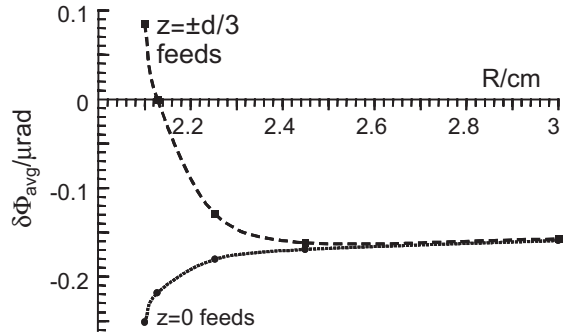

Figure 9. $\delta\Phi_{\text{avg}}$ as a function of cavity radius, R, for cavities that are fed at $z = 0$ and $z = \pm d/3$. These cavities have below-cutoff waveguide sections as in figure 8, and these ensure that the phase shifts are everywhere small. For cavities fed at the midsection, $z = 0$, $\delta\Phi_{\text{avg}}$ is negative for all R. With power feeds at $z = \pm d/3$, the $m = 0$, $p = 3$ phase shifts offset the $m = 0$, $p = 1$ phase shifts. The $m = 0$, $p = 3$ mode has a larger effect for small R and opposite effects for $z = 0$ and $z = \pm d/3$ feeds. For $R = 2.128$ cm and feeds at $z = \pm d/3$, the cavity in figure 8, $\delta\Phi_{\text{avg}} = 0$.

therefore we take the lowest order variation to be quadratic, $n(r) = (N/\pi r_a^2)\,[1 + \alpha(r^2/r_a^2 - 1/2)]$, where α gives the curvature. For all clocks, α should be small and negative during the first cavity traversal and negligible during the second. We take the difference of $\delta\Phi_{\text{eff}}(r)$ on the two cavity passages, which leaves an $m = 0$ average effective phase difference of $\delta\Phi_{\text{avg}} = \int_0^{r_a} \delta\Phi_{\text{eff}}(r)(2r^2/r_a^4 - 1/r_a^2) r\,\mathrm{d}r$. For the cavity design in figure 8, $\delta\Phi_{\text{avg}} = 0$ and the variation of $\delta\Phi_{\text{eff}}(r)$ is less than ±0.1 μrad[5]. In figure 9, we show the $\delta\Phi_{\text{avg}}$ we get from finite element calculations for several cavity radii where the cavities are fed at $z = 0$ and $z = \pm d/3$. As mentioned above, while the cavity with no endcap holes in figure 7 has a large positive $m = 0, p = 1$ effective phase shift difference for large R, the effects of the endcap holes and 2.1 cm diameter below-cutoff waveguide sections prevent $\delta\Phi_{\text{avg}}$ from increasing for large R. Feeding a cavity at $z = \pm d/3$, versus $z = 0$, excites the $p = 3$ mode with an opposite polarity and twice the amplitude—the effect of the $m = 0$, $p = 3$ mode is clear in figure 9 for cavity radii near 2.1 cm to 2.2 cm.

5. Summary

We have shown an analytic solution for the phase variations that occur in the microwave cavities used in atomic clocks. The analytic solutions show significant new terms that are not present in previous two-dimensional treatments. These terms show that cavities with radii near $R = 2.1$ cm have smaller phase shifts. We have shown that a series of two-dimensional finite element solutions is efficient and can accurately calculate the three-dimensional phase variations in microwave cavities. We have applied the finite element method to the cavities with endcap holes. Our analytic solutions guide us to an improved cavity where the peak phase shifts that the atoms experience are 1000 times smaller than those for cavities currently in use. The effective phase shift variations are less than ±0.1 μrad, and, with reasonable assumptions about density anomalies, the average phase shift is vanishingly small.

[5] This design retains $\delta\Phi_{\text{avg}} = 0$ when the scale is changed as $1/\omega$, e.g. to construct a cavity resonant at 6.834 GHz for ^{87}Rb clocks.

Acknowledgments

We gratefully acknowledge stimulating discussions with Wenhua Yu and financial support from the NASA Microgravity program, the Office of Naval Research, and Penn State University.

Appendix

Here, we give the remaining field components of equation (5) for the small standing wave field, $\vec{f}(\vec{r})$ and $\vec{g}(\vec{r})$, for the case of sidewall losses:

$$\begin{aligned}
\vec{g}(\vec{r}) &= \sum_{m=0}^{\infty}\sum_{p=1+\delta_{m,0}}^{\infty}\vec{g}_{m,p}(\vec{r}),\\
f_{r,m,p}(\vec{r}) &= \mu_0\omega\frac{\delta k_1}{2\gamma_p}\frac{m}{r}\frac{1-(-1)^p}{2}\frac{J_0(\gamma_1 R)}{J'_m(\gamma_p R)},\\
&\quad\times J_m(\gamma_p r)\sin(m\phi)\cos(k_p z)\\
f_{\phi,m,p}(\vec{r}) &= \mu_0\omega\frac{\delta k_1}{2}\quad\frac{1-(-1)^p}{2(1+\delta_{m,0})}\frac{J_0(\gamma_1 R)}{J'_m(\gamma_p R)}\\
&\quad\times J_m'(\gamma_p r)\cos(m\phi)\cos(k_p z),\\
g_{r,m,p}(\vec{r}) &= \frac{\delta k_1 k_p}{2}\frac{1-(-1)^p}{2(1+\delta_{m,0})}\frac{J_0(\gamma_1 R)}{J'_m(\gamma_p R)}\\
&\quad\times J'_m(\gamma_p r)\cos(m\phi)\sin(k_p z),\\
g_{\phi,m,p}(\vec{r}) &= -\frac{\delta k_1 k_p}{2\gamma_p}\frac{m}{r}\frac{1-(-1)^p}{2}\frac{J_0(\gamma_1 R)}{J'_m(\gamma_p R)}\\
&\quad\times J_m(\gamma_p r)\sin(m\phi)\sin(k_p z).
\end{aligned}\tag{A1}$$

The sum over m and p for each component is the same as in equation (5) and, because the primary electric field is transverse, $\vec{f}(\vec{r})$ is transverse and $f_{z,m,p}(\vec{r}) = 0$. For endcap losses, equations (A1) are multiplied by $2k_1^2R/\gamma_1^2 d$.

The remaining non-zero $m = 0$, $p = 1$ field components following equation (10) for endcap losses are

$$\begin{aligned}
f_{\phi,0,1}(r,z) &= \mu_0\omega\frac{\delta}{2d}\frac{k_1^2}{\gamma_1^2}[k_1 r J_0(\gamma_1 r)\cos(k_1 z)\\
&\quad+\gamma_1 z J_1(\gamma_1 r)\sin(k_1 z)] - \frac{\delta}{2d}E_{0,\phi}(r,z),\\
g_{r,0,1}(r,z) &= \frac{\delta}{2d}\frac{k_1^3}{\gamma_1^2}[k_1 r J_0(\gamma_1 r)\sin(k_1 z) - \gamma_1 z J_1(\gamma_1 r)\\
&\quad\times\cos(k_1 z)] + \frac{\delta}{d}\left(\quad-\frac{3}{2}\right)H_{0,r}(r,z).
\end{aligned}\tag{A2}$$

References

[1] See for example Marion H *et al* 2003 Search for variations of fundamental constants using atomic fountain clocks *Phys. Rev. Lett.* **90** 150801
Jefferts S R *et al* 2002 Accuracy evaluation of NIST-F1 *Metrologia* **39** 321–36
Swanson T B, Burt E A and Ekstrom C R 2002 Characterization of the USNO cesium fountain *Proc. 6th Symp. on Frequency Standards Metrology* ed P Gill (Singapore: World Scientific) pp 80–7
Bauch A, Schröder R and Weyers S 2003 Discussion of the uncertainty budget and of long term comparison of PTB's primary frequency standards CS1, CS2 and CSF1 *Proc. 2003 IEEE Int. Frequency Control Symp. and 17th E. F. T. F.* pp 191–9
Szymaniec K, Chalupczak W and Henderson D 2003 Initial evaluation of the NPL caesium fountain frequency standard *Proc. 2003 IEEE Int. Frequency Control Symp. and 17th E. F. T. F* pp 112–14
Kurosu T, Fukuyama Y, Abe K, Yanagimachi S and Koga Y 2003 Evaluation of the Cs atomic fountain frequency standard at NMIJ/AIST *Proc. 2003 IEEE Int. Frequency Control Symp. and 17th E. F. T. F.* pp 123–6
Levi F, Lorini L, Calonico D, Bertacco E K and Godone A 2003 IEN-CsF1 Accuracy evaluation and two way frequency comparison *Proc. 2003 IEEE Int. Frequency Control. Symp. and 17th E. F. T. F.* pp 199–204
[2] Bauch A, Heindorff T and Schroeder R 1985 Measurement of the frequency shift due to distributed cavity phase difference in an atomic clock *IEEE Trans. Instrum. Meas.* **34** 136–8
[3] Vecchi G and DeMarchi A 1993 Spatial phase variations in a TE011 microwave cavity for use in a cesium fountain primary frequency standard *IEEE Trans. Instrum. Meas.* **42** 434–8
[4] Khursheed A, Vecchi G and DeMarchi A 1996 Spatial variations of field polarization and phase in microwave cavities: application to the cesium fountain cavity *IEEE Trans. UFFC* **43** 201–10
[5] Jefferts S R, Drullinger R E and DeMarchi A 1998 NIST cesium fountain microwave cavities *Proc. 1998 Frequency Control Symp.* pp 6–8
[6] Laurent Ph, LeMonde P, Abgrall M, Santarelli G, Pereira Dos Santos F, Clairon A, Petit P and Aubourg M 1999 Interrogation of cold atoms in a primary frequency standard *Proc. 1999 Joint Meeting EFTF and Frequency Control Symp.* pp 152–5
[7] See for example Ashby N, Römisch S and Jefferts S R 2003 Endcaps for TE_{01} cavities in fountain frequency standards *Proc. Frequency Control Symp.* pp 1076–83
[8] Davies J B, Fernandez F A and Philippou G Y 1982 Finite element analysis of all modes in cavities with circular symmetry *IEEE Trans. Microwave Theory Tech.* **82** 1975–80
See also Britt C L 1989 Solution of electromagnetic scattering problems using time domain techniques *IEEE Trans. Antenna Propagat.* **37** 1181–92
Chen Y, Mittra R and Harms P 1996 Finite-difference time-domain algorithm for solving Maxwell's equations in rotationally symmetric geometries *IEEE Trans. Microwave Theory Tech.* **44** 832
[9] Fertig C, Li R, Rees J I and Gibble K 2002 Distributed cavity phase shifts and microwave photon recoils *Proc. 2002 IEEE Frequency Control Symp.* pp 469–72
[10] See Bickford W B 1994 *A First Course in the Finite Element Method* 2nd edn (Burr Ridge: Irwin) p 138
[11] Santarelli G, Laurent P, Clairon A, Dick G J, Greenhall C A and Audoin C 1996 Theoretical description and experimental evaluation of the effect of the interrogation oscillator frequency noise on the stability of a pulsed atomic frequency standard *Proc. European Frequency Time Forum* vol 45, pp 66–71
[12] Lemonde P, Santarelli G, Laurent Ph, Pereira F, Clairon A and Salomon Ch 1998 The sensitivity function: a new tool for the evaluation of frequency shifts in atomic spectroscopy *Proc. Frequency Control Symp.* pp 110–15
[13] Audoin C and Vanier J 1989 *The Quantum Physics of Atomic Frequency Standards* (Bristol: Adam Hilger) p 620
[14] Clairon A, Laurent P, Santarelli G, Ghezali S, Lea S N and Bahoura M 1995 A cesium fountain frequency standard: preliminary results *IEEE Trans. Instrum. Meas.* **44** 128–31
[15] Fertig C, Bouttier J and Gibble K 2000 Laser-cooled Rb clock *Proc. 2000 IEEE Frequency Control Symp.* pp 680–6